LA-5532-MS

INFORMAL REPORT

Plasma Chemistry and the Dynamics of Carbon Foils Irradiated by High Intensity Laser Pulses

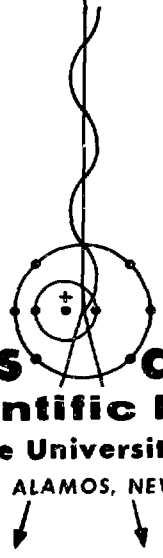

los alamos
scientific laboratory
of the University of California
LOS ALAMOS, NEW MEXICO 87544

UNITED STATES
ATOMIC ENERGY COMMISSION
CONTRACT W-7405-ENG. 36

In the interest of prompt distribution, this LAMS report was not edited by the Technical Information staff.

Printed in the United States of America. Available from
National Technical Information Service
U. S. Department of Commerce
5285 Port Royal Road
Springfield, Virginia 22151
Price: Printed Copy $4.00; Microfiche $1.45

LA-5532-MS
Informal Report
UC-20

REPORTING DATE: February 1974
ISSUED: March 1974

los alamos
scientific laboratory
of the University of California
LOS ALAMOS, NEW MEXICO 87544

Plasma Chemistry and the Dynamics of Carbon Foils Irradiated by High Intensity Laser Pulses

by

S. D. Rockwood

PLASMA CHEMISTRY AND THE DYNAMICS OF CARBON FOILS IRRADIATED BY HIGH INTENSITY LASER PULSES

by

S. D. Rockwood

ABSTRACT

Calculations are presented which display the temporal behavior of electron and ion temperatures and ion number densities during the evolution of a carbon plasma irradiated by an intense laser pulse. These plasma kinetics calculations are coupled with a one dimensional Lagrangian hydrocode simulation of the disassembly of thin carbon foil targets. Results of these calculations show line radiation from the targets to be negligible for incident fluxes $\phi \geq 10^{14}$ watts/cm^2 while bound free radiation represents the dominant radiation loss in many cases of interest. From the results of the numerical calculations an analytic model is developed which predicts the experimentally observed dependence of transmission through thin targets as a function of laser and target parameters.

I. INTRODUCTION

This report is divided into three sections. The first section examines the detailed kinetics involved in the laser induced formation of a carbon plasma. In the second section this analysis is incorporated into a one dimensional Lagrangian hydrocode to simulate the ionization and disassembly of thin carbon targets irradiated by 1.06μ Nd-glass laser radiation. From the numerical solutions of Section III certain approximations are observed to be justified which allow one to derive an analytic expression for the transmission of the carbon foils as a function of laser and material parameters. In Section IV the analytic results are compared with experimental data and excellent agreement is observed over a wide range of thicknesses for both carbon and cellulose acetate targets.

II. CARBON PLASMA CHEMISTRY

A. Physical Processes

The kinetics of plasma formation are examined through numerical solution of the coupled rate equations governing the electron and ion temperatures, the number density of species in each charge state and the populations of selected excited states. The physical processes considered include: heating of the electrons through absorption of laser light, electron production through cascade ionization, electron impact excitation, radiative recombination, three body recombination, line radiation with possible corrections for resonant trapping, bremsstrahlung and free-bound radiation. When the electron density is below the critical density for the incident wavelength, heating of the electrons is assumed to proceed through inverse bremsstrahlung using the absorption coefficient of Dawson.[1] When the electron density exceeds the critical density a classical skin depth absorption coefficient is employed.[2] As sources of input data the hydrogenic model of Seaton is used for radiative recombination,[3] the cross sections of Lotz[4] for impact ionization and the cross sections of Moiseiwitsch and Smith for impact excitation.[5] These cross sections are generally applicable to any atomic system if the energy levels and optical oscillator strengths are known. For most materials of interest the required data are available from Refs. (6) and (7). The three body recombination rates are derived from the ionization rates by requiring these two processes to yield a Saha equilibrium.

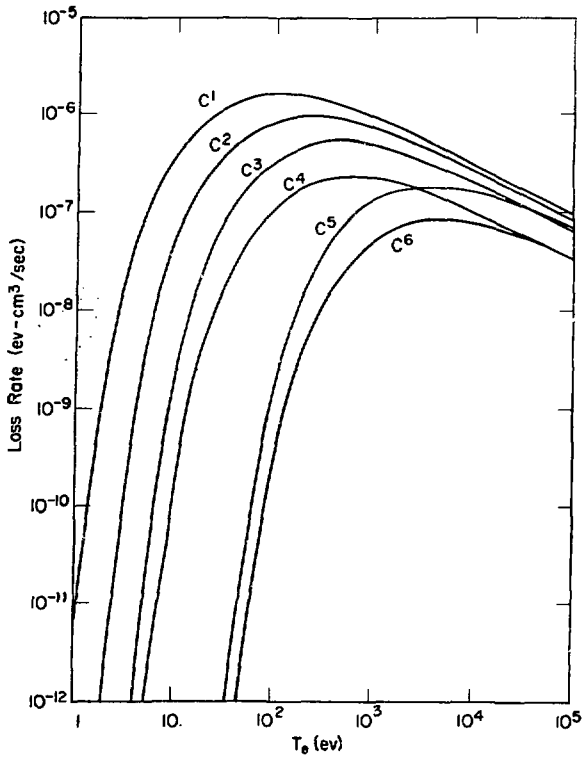

Fig. 1a. Electron energy loss rates for ionization of various carbon ions as a function of electron temperature.

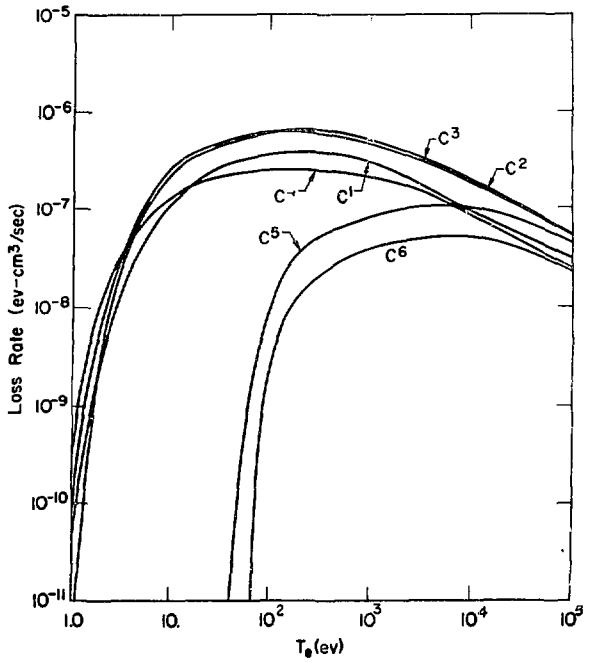

Fig. 1b. Electron energy loss rates through excitation of selected levels in various carbon ions as a function of electron temperature. The calculations follow excitation of each of the levels listed below individually however for simplicity in graphing these have been combined into a lumped rate for each ion. The levels considered are: C^{I}, 2p3d, 2p3s; C^{II}, $2s2p^2(^2D)$, $2s2p^2(^2P)$, 2s3d; C^{III}, 2s2p, 2s3p; C^{IV}, 2p, 3p; C^{V}, 1s2p, 1s3p, C^{VI}, 2p.

Figures (1a) and (1b) display the energy loss rates per electron and per atom derived from the above data for ionization and excitation of the various charge states of carbon.

B. Plasma Constituents

Using the method of Fowler and Warten[8] for integration of the coupled rate equations we have studied both laser and electron beam heating of solid carbon targets. The typical results of such a calculation are shown in Figures (2a-b). In Fig. (2a) observe that the electron temperature rises rapidly to a quasi-equilibrium value of $T_e = 6$ ev where the energy input is balanced by ionization losses in C^{I} obtainable from Fig. (1a). By a time of $t = 10^{-12}$ sec most of the C^{I} has been ionized. The temperature now rises rapidly due to the lower loss rates in higher charge states of carbon (see Fig. 1a) and further stripping of the various charge states proceeds rapidly until C^{VII} becomes the dominant ion for $t > 10^{-11}$ sec. The calculation presented in Fig. (2) is of particular interest because an inversion is seen to develop between the 1s2p and 1s3p levels of C^{V} for times 2×10^{-12} sec $\leq t \leq 3 \times 10^{-11}$ sec , see Fig. (2b). This inversion results from very rapid three-body recombination preferentially populating the higher 1s3p level.

C. Radiation

Laser fluxes of interest here are always 10^{13} watts/cm^2 or greater in which case most of the computed radiation from the plasma is free-bound radiation resulting from radiative recombination. As the electron temperature increases beyond $T_e \approx 5$ kev bremsstrahlung radiation becomes dominant. In all cases line radiation plays an insignificant role as

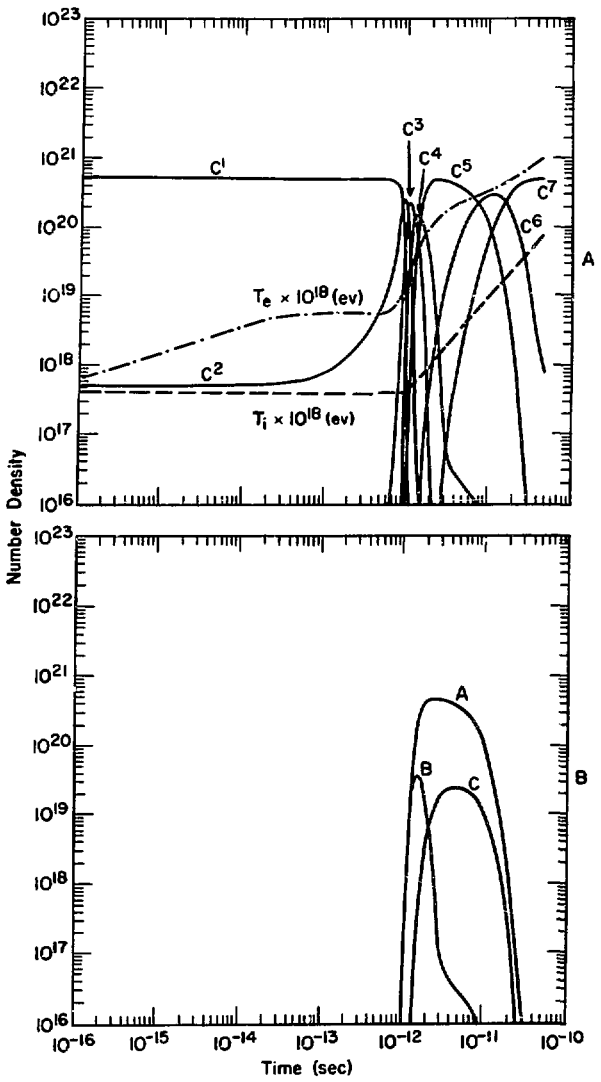

Fig. 2a. Calculated electron and ion temperature and ground state populations of carbon ions as a function of time.

Fig. 2b. Ground state and excited state populations as a function of time for C^V. Level notation, A = ground state $1s^2$, B = 1s2p, C = 1s3p.

an energy loss since nearly all electrons which might radiate are removed through ionization on a time scale short compared to their radiative lifetimes. Only when the incident flux is on the order of 10^{12} watts/cm^2 or less does line radiation have a chance to play a significant role. With laser fluxes in this low range, $T_e \lesssim 3$ ev ionization rates can become comparable to, or slower than impact excitation followed by radiative relaxation. If the target is then small enough to be optically thin in the lines, line radiation may represent a large energy loss for the plasma. As mentioned previously this low flux case is not of interest in the present investigation. Figure (3) shows various contributions to a typical computed radiation spectrum from an optically thin target at a temperature of $T_e = 664$ ev. The characteristic sawtooth behavior of the free-bound contributions is of interest since it may represent a useful diagnostic on plasma

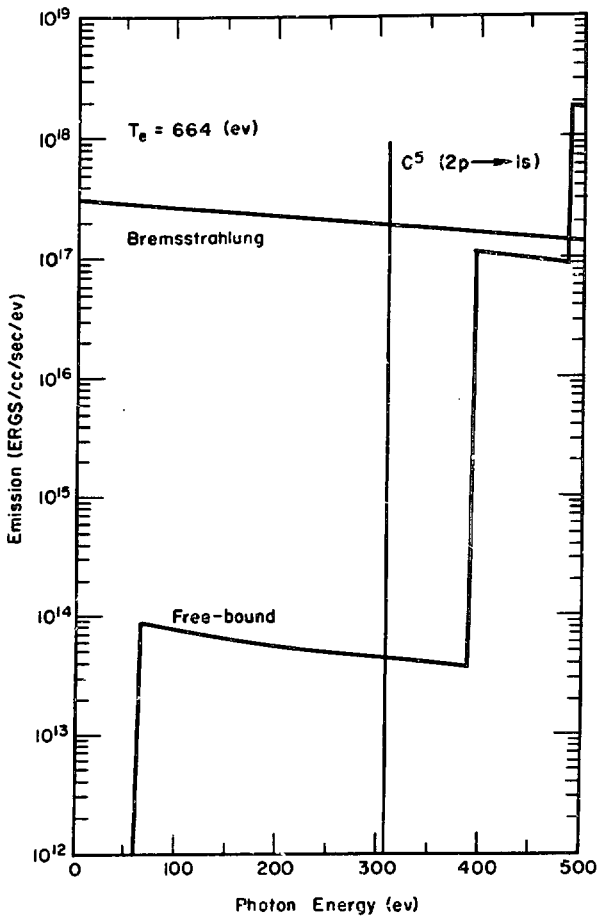

Fig. 3. Contributions to the total plasma emission spectrum.

conditions. The energies at which the spectrum rises abruptly are the ionization potentials of the charge states of carbon and give an indication of the ions present, while the decrease in the spectrum above the ionization potential is principally due to the Boltzmann factor in the electron distribution and hence may be used to determine the electron temperature.

III. TARGET DYNAMICS

A. Physical Processes

The temporal evolution of the target density, velocity, and pressure are described through numerical solution of their Lagrangian equations of motion using a quadratic artificial viscosity.[9] An ideal gas equation of state is assumed with an isentropic exponent of $\gamma = 5/3$. The thermal pressure is augmented by a magnetic pressure with the local magnetic field determined by

$$B(X,T) = \sqrt{4\pi\phi(x,t)/V(x,t)}$$

where $\phi(x,t)$ is the laser flux with frequency ω and $V(x,t) = c\sqrt{1 - \omega_p^2/\omega^2}$ is the group velocity. Values for $V(x,t)$ are bounded below by $V(x,t) \geq .1c$. It should be noted that the inclusion of this term in the hydrodynamic equations has not significantly altered the results for experiments of interest here.

The behavior of the plasma constituents in each computational cell is described through the solution of their coupled rate equations as described in Section II. Electron temperatures are also coupled in space through non-linear thermal conduction using the thermal conduction coefficient given in Ref. (10). Both the thermal conduction and plasma chemistry equations are integrated using an explicit integration algorithm and subcycled over the chosen time step if it exceeds their own characteristic times. For the cases of interest here the targets are quite thin with thicknesses $\lesssim 10^{-5}$ cm hence radiation transport has been neglected and the material is assumed to be optically thin to all internal radiation discussed in Section II.

B. Results

Figures (4-6) display the typical behavior of a thin target of carbon irradiated by a 25 picosecond pulse of 1.06 μ radiation at an average power level of 10^{16} watts/cm^2. The target has a thickness of 5×10^{-6} cm and a density of 2 gm/cm^2 for a mass per unit area of 10 μgm/cm^2. From Fig. (4a-b) one may observe that the target is fully ionized long before any hydrodynamic motion begins. In subsequent figures the target is seen to expand with the electrons exerting all the pressure. Electrons and ions

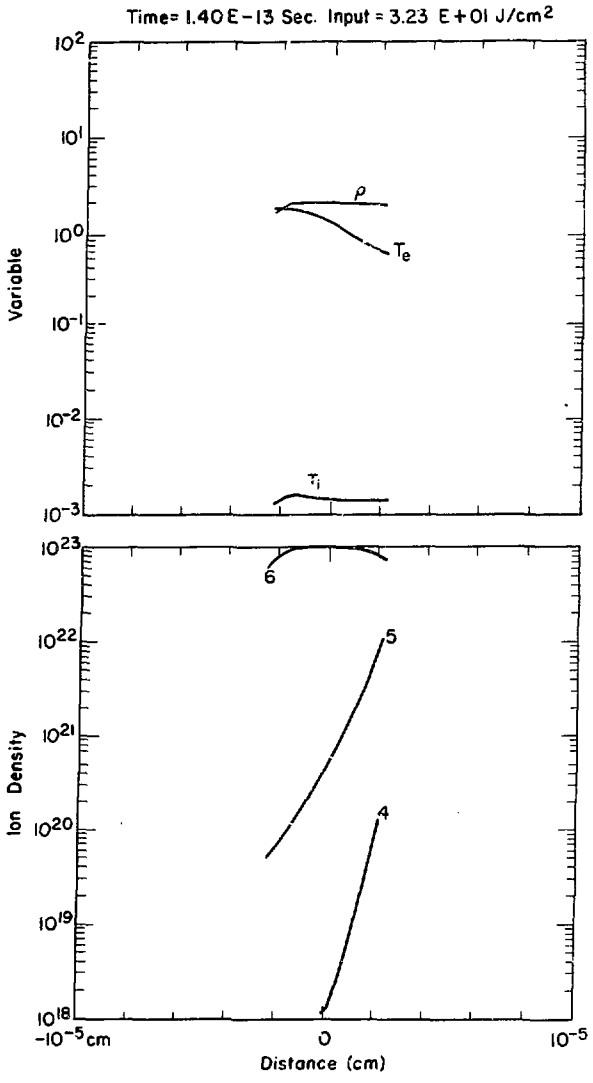

Fig. 4a. Density (gm/cm^3), electron temperature (kev), pressure x 10^{-15} dynes/cm^2, and ion temperature (kev) as a function of distance at a time of 1.4 x 10^{-13} sec for a 10 μgm/cm^2 carbon foil irradiated with 2.5 x 10^5 joules/cm^2 in a 25 picosecond Gaussian pulse shape.

Fig. 4b. Ground state ion densities as a function of distance with the same laser conditions as Fig. (4a).

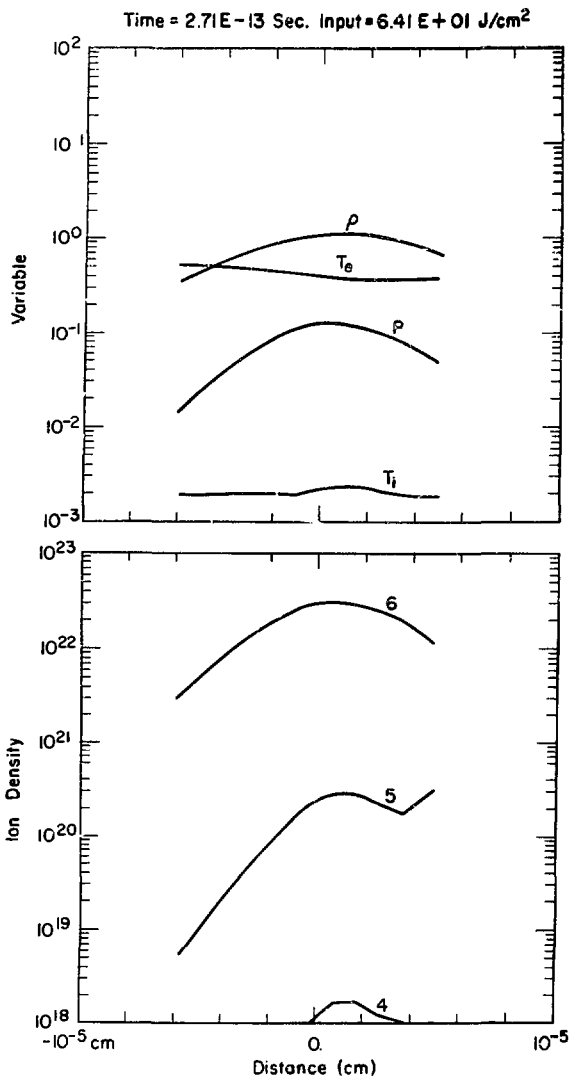

Fig. 5a. Same quantities and conditions as Fig. (4a) at a time of 2.7×10^{-13}.

Fig. 5b. Same quantities as Fig. (4b) at 2.7×10^{-13} sec.

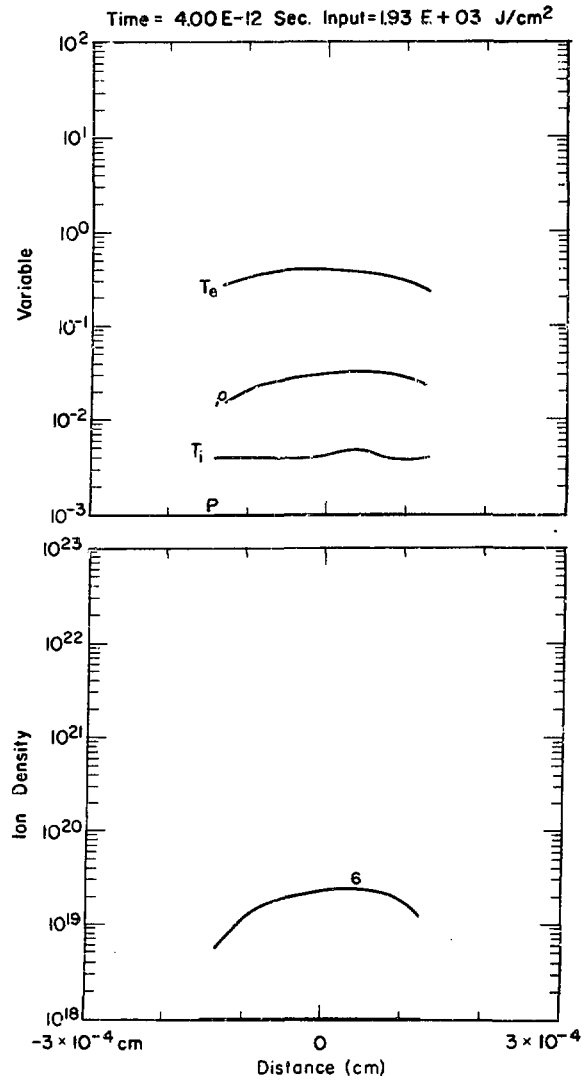

Fig. 6a. Same quantities and conditions as Fig. (4a) at a time of 4×10^{-12}.

Fig. 6b. Same quantities as Fig. (4b) at 4×10^{-12} sec.

are accelerated to a velocity of approximately 4×10^7 cm/sec however note that the ions remain thermally cold with $T_i \lesssim 5$ ev. This is a consequence of decreases in the density on a time scale faster than the electron-ion coupling time. As a result of the low value for T_i ion detectors should record sharp signals for fast ions with a narrow thermal spread.

Another interesting feature is that while the electron temperature drops from $T_e \approx 1$ kev to $T_e \approx 400$ ev during the expansion little recombination takes place owing to the decreased ion and electron densities. Hence the charge distribution is frozen out of equilibrium and C^{VII} formed at very early times is always the dominant ion.

By a time of $t = 8 \times 10^{-12}$ sec, (Fig. 6) the target density has dropped below the critical density for 1.06 μ light and all subsequent radiation is transmitted with very little attenuation. This is demonstrated in Fig. (7) which displays the computed time dependent transmission of the target. Initially, the solid is overdense and the laser light is attenuated with a classical skin depth as described in Sec. II. As the target begins to expand it initially remains overdense and the increasing thickness leads to the decrease in transmission seen for $10^{-13} \leq t \leq 4 \times 10^{-13}$ sec. By a time of 10^{-12} seconds the target begins to go underdense resulting in the rapid increase in transmission which approaches 100% by $t = 8 \times 10^{-12}$ sec. Subsequent dynamics of the system are uninteresting with the material expanding nearly adiabatically and absorbing very little energy from the laser.

From calculations like those presented above it is possible to make several observations about the behavior of these thin targets. First, the material is always ionized essentially instantaneously and then frozen into this state by subsequent expansion. Secondly the material accelerates rapidly to a terminal velocity which remains constant for the duration of the expansion. Finally, the transmission remains very nearly zero for even the thinnest targets until they become underdense at which time it increases rapidly to 100%. With these facts in mind it is possible to develop the following model for transmission as a function of material and laser parameters which may be compared with experiments.

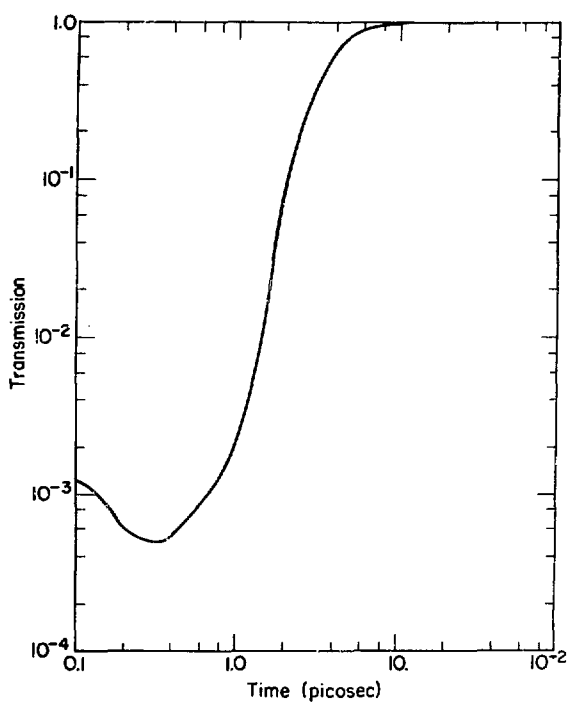

Fig. 7. Computed transmission as a function of time for problem conditions displayed in Figs. (4-6).

IV. ANALYTIC RESULTS

Similarity solutions for an isothermal expansion in a planar geometry[12] show that the density ρ, is given by

$$\rho = \rho_o e^{-(x/\xi_o)^2} = \frac{\mu}{\sqrt{\pi}\xi_o} e^{-(x/\xi_o)^2} \tag{1}$$

where μ is the initial mass per unit area and the scale length as a function of time is

$$\xi_o = \sqrt{\frac{32}{45}} \left(\frac{W}{\mu}\right)^{1/2} t^{3/2} \tag{2}$$

for the special case of a constant power input per unit area, W. Now define t_c as the time at which the initial solid density has decreased to the critical density.

$$\rho_c(\mathrm{gm/cm^3}) = \frac{1.85 \times 10^{-3}}{\lambda^2} \left(\frac{A}{Z}\right) \tag{3}$$

where λ is the laser wavelength in microns, A is the atomic weight of the target, and Z its atomic number. Then from Eq. (1) and (2)

$$\rho(x = 0, t) = \sqrt{\frac{45}{32\pi}} \frac{1}{W} \left(\frac{\mu}{t}\right)^{3/2} \tag{4}$$

and using Eq. (3) along with the definition of t_c yields

$$t_c = \left(\frac{45}{32\pi}\right)^{1/3} \left(\frac{1}{W}\right)^{1/3} \frac{\mu}{\rho_c^{2/3}} \tag{5}$$

For thin targets the average power deposited per unit area is related to the average incident laser flux ϕ (ergs/cm^2/sec) by

$$W = \alpha \phi d \tag{6}$$

where $\alpha(cm^{-1}) = \sqrt{\omega_p^2 - \omega^2}/c$ is the attenuation length in the overdense material and $d = \mu/\rho$ is the target thickness. Thus substituting Eq. (6) into Eq. (5) and using Eq. (3) yields

$$t_c(sec) = 50.7\left(\frac{\rho}{\alpha\phi}\right)^{1/3} \lambda^{4/3}\left(\frac{Z}{A}\right)^{2/3} \mu^{2/3} \qquad (7)$$

where the wavelength λ is in microns, (Z/A) in atomic units, and all other quantities are in C.G.S. units.

The transmission, T, will now be defined as the fraction of the total energy incident for times $t > t_c$, i.e.

$$T = \int_{t_c}^{\infty} \phi(t)\, dt \Big/ \int_0^{\infty} \phi(t)dt. \qquad (8)$$

If at this point one assumes a Gaussian pulse profile $\phi(t) = \phi_o \exp(-t^2/\tau^2)$ then Eqs. (7) and (8) give

$$T = 1 - erf(y) \qquad (9)$$

where erf (y) is the error function[11] and

$$y \equiv \frac{t_c}{\tau} = 50.7\left(\frac{\rho}{\alpha\phi}\right)^{1/3} \lambda^{4/3} \left(\frac{Z}{A}\right)^{2/3} \mu^{2/3} \frac{1}{\tau} \qquad (10)$$

From Eqs. (9) and (10) one may observe that the transmission is most sensitive to the laser parameters λ and τ while the most important material parameter is μ. Inserting values appropriate to the conditions of the cellulose acetate experiments from Ref. (13); $\lambda = 1.06$ μm, $\rho = 1.5$ gm/cm^2, $Z/A = .53$, $\alpha = 1.3 \times 10^6$ cm^{-1}, $\phi = 10^{23}$ ergs/cm^2/sec, and choosing $\tau = 3.9 \times 10^{-12}$ sec to predict 3% transmission at $\mu = 2 \times 10^{-5}$ gm/cm^2 yields the points indicated by open circles in Fig. (8) compared to the experimental data (solid line). This value of τ required by Eq. (10) to fit the experimental data corresponds to a FWHM pulse length of 5.4×10^{-12} sec and is shorter than the nominal experimental value of 25×10^{-12} sec as determined by two photon flourescence. The situation is similar for the carbon foil experiments of Ref. (13) as indicated in Fig. (9) however in this case the scatter in experimental data as bounded by the two solid lines is greater.

The most striking feature of Eq. (9) is that it accurately predicts the observed functional dependence of T upon μ for both experiments. Its quantitative error which requires one to normalize to a pulse width shorter than the observed experimental

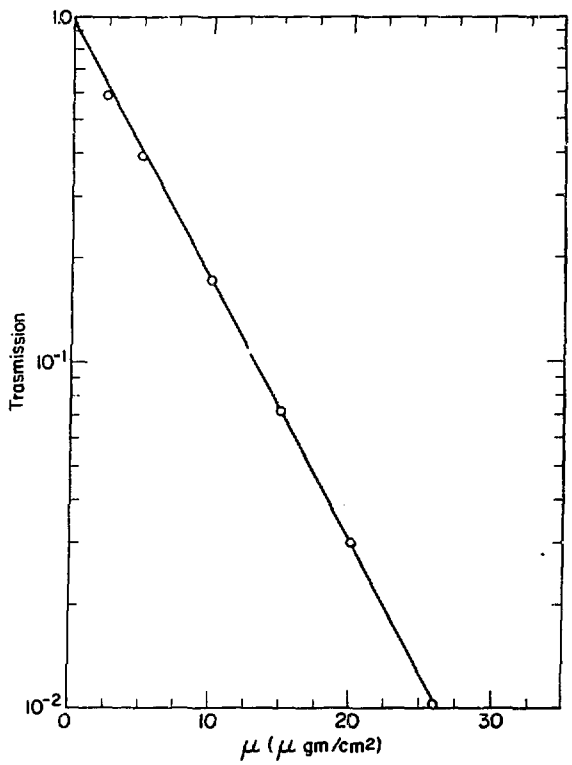

Fig. 8. Experimentally measured transmission (solid line) of cellulose acetate foils as a function of foil thickness. Open circles are calculated from Eq. (8) using $\tau = 3.9 \times 10^{-12}$ sec.

value may be qualitatively explained by the assumption of an instantaneous rise time in obtaining the similarity solution for ρ, Eq. (1). An alternative explanation which is also qualitatively correct is to assume significant laser absorption is occurring at sub-critical densities. In particular in the present case if one assumes the material must expand to slightly less than 1/4 ρ_c then the value of τ required to fit the data can be brought into agreement with the experimentally measured value. While such an explanation is in line with current absorption simulations[14] a word of caution is in order since the experimental measurement of τ and the analytic model developed above may each be in error by as much as a factor of two.

The important observation to make is that Eq. (9) correctly describes the currently available

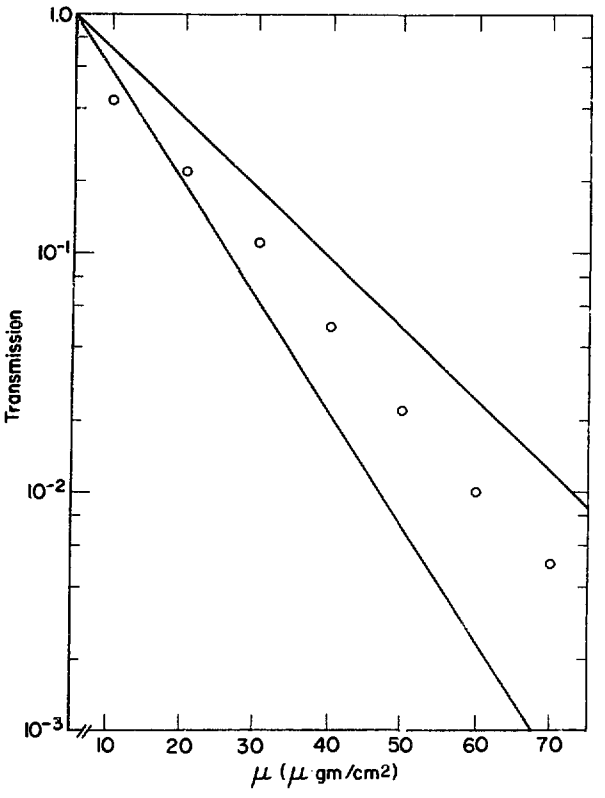

Fig. 9. Experimentally measured transmission data bounded by solid lines as a function of thickness for carbon foils. Open circles are calculated from Eq. (8) using $\tau = 5.5 \times 10^{-12}$ sec. Note the suppressed zero on the thickness scale.

data and suggests further experiments with varied laser pulse widths and wavelengths to check the predicted dependence of T upon these parameters.

REFERENCES

1. Johnston, T. W. and J. M. Dawson, Phys. Fluids, 16, 722 (1973).
2. Jackson, J. D., Classical Electrodynamics, John Wiley, New York (1962).
3. Seaton, M. J., Mon. Not. Roy Astrom. Soc. 119, 81 (1959).
4. Lotz, W. Ast. Phys. J. 14, 207 (1967).
5. Moiseiwitsch, B. L. and S. J. Smith, Rev. Mod. Phys. 40, 238 (1968).
6. Wiese, W. L., M. W. Smith and B. M. Miles, Atomic Transition Probabilities, NSRDS-NBS 22 (1969).
7. Moore, C. E., Atomic Energy Levels NBS-467 (1958).
8. Fowler, M. E. and R. M. Warten, IBM J. Res. Dev. 11, 537 (1967).
9. Richtmyer, R. D. and K. W. Morton, Difference Methods for Initial Value Problems, Wiley (Interscience), New York (1967).
10. Spitzer, L., Jr., Physics of Fully Ionized Gases, Wiley (Interscience), New York (1967).
11. Handbook of Mathematical Functions..., ed. M. Abramowitz and I. A. Stegun, NBS Applied Math Series 55 (1964).
12. Morse, R. and S. Rockwood (to be published).
13. Giovanielli, D. B., R. P. Godwin, and G. H. McCall, Bull. Am. Phys. Soc. 18, 1255 (1973).
14. Forslund, D. W., J. M. Kindel and E. L. Lindman, Phys. Rev. Lett. 30, 739 (1973).